Polymer Chemistry

Cite this: *Polym. Chem.*, 2012, **3**, 3100

www.rsc.org/polymers

PAPER

Complementary multiple hydrogen bonding interactions mediate the self-assembly of supramolecular structures from thymine-containing block copolymers and hexadecyladenine

Yi-Chen Wu and Shiao-Wei Kuo*

Received 6th April 2012, Accepted 23rd May 2012
DOI: 10.1039/c2py20197f

In this study we used nitroxide-mediated radical polymerization to synthesize poly(styrene-*b*-4-vinylbenzyl azide) (PS-*b*-PVBN$_3$) and then used click chemistry to react it with propargyl-thymine (PT) to obtain a series of thymine (T)-containing block copolymers, poly(styrene-*b*-4-vinylbenzyl triazolylmethyl methylthymine) (PS-*b*-PVBT). We then added an amphiphilic surfactant, hexadecyladenine (A-C16), to complex with the PVBT units in the PS-*b*-PVBT copolymers through complementary multiple hydrogen bonding interactions. The resulting supramolecular comb–coil diblock copolymers formed lamellae-within-lamellae self-assembled structures, with PS lamellar domains (diameter: *ca.* 20–25 nm) in a matrix consisting of lamellar mesophases (lamellar inter-distance: *ca.* 2.3 nm) organized by the PVBT/A-C16 complex. Fourier transform infrared spectroscopy provided evidence for multiple hydrogen bonding between the A-C16 and T groups of the PS-*b*-PVBT copolymers. The small-angle X-ray scattering patterns of these self-assembled supramolecular systems were very temperature-sensitive. A striking feature was the appearance of the ordered scattering of the lamellar structure at temperatures higher than the melting point of A-C16 (>120 °C), with A-C16 becoming fully miscible with both the PS and PVBT phases at higher temperature; A-C16 was miscible only with the PVBT domains at room temperature, thereby influencing the volume fraction of the PS segment.

Introduction

Self-assembled supramolecular structures have attracted great interest because of their potential applications as functional materials.[1–3] In general, the self-assembly of hierarchical nanostructures from ABC triblock copolymers can lead to three-phase lamellae, core–shell cylinders, and other hierarchical structures.[4] Although the syntheses of ABC triblock copolymers can be complicated, mixing A-*b*-B and C-*b*-D copolymers is a relatively simple method for preparing similar self-assembled morphologies.[5–7] Typically, for such systems, the B and C segments should be attracted through intermolecular interactions (*e.g.*, hydrogen bonding,[8–13] electrostatic interactions,[14,15] metal–ligand coordination[16]), while the A and D block segments should be incompatible or immiscible.

In addition to the self-assembly of ABC triblock copolymers or mixtures of A-*b*-B and C-*b*-D diblock copolymers, the groups of Ikkala and ten Brinke initiated studies of the bulk state properties of comb-shaped supramolecular systems formed through hydrogen bonding of short flexible side chains in diblock copolymers. They interacted poly(styrene-*b*-4-vinylpyridine) (PS-*b*-P4VP) through hydrogen bonds to an oligomeric amphiphile [*e.g.*, nonadecylphenol (NDP), pentadecyl phenol (PDP)][17–20] to form lamellar-within-lamellar, lamellar-within-cylinder, and lamellar-within-spherical self-assembled supramolecular structures.[21] This supramolecular method for synthesizing materials with two different length scales from a functional block copolymer and a suitable oligomeric amphiphile, using hydrogen bonding interactions, results in so-called hydrogen-bonded comb–coil block copolymers.[17–21] Here, one block is a comb-like polymer–amphiphile complex and the other is a coil-like polymer. The hierarchical self-assembly of such supramolecular structures arises from highly organized microphase-separated structures derived from the AB diblock copolymers (within the 10–100 nm range) and organization, at a much smaller length scale (2–6 nm), of the hydrogen-bonded polymer–amphiphile complexes.[17–21] This shortened scale is determined by the length of the repulsive side chains within the comb block and the moieties attached through noncovalent bonds (*e.g.*, hydrogen bonding, ionic interactions, coordination). In general, these interactions have been formed through single-site hydrogen bonding of the OH groups of PDP and the pyridyl groups of P4VP, but they are relatively weaker than the multiple hydrogen bonding interactions formed in DNA-like complexes [*e.g.*,

Department of Materials and Optoelectronic Science, National Sun Yat-Sen University, Kaohsiung, 804, Taiwan. E-mail: kuosw@faculty.nsysu.edu.tw

adenine (A) interacting with thymine (T) or guanine (G) with cytosine (C)].[22–25]

Mimicking molecular recognition in biological system is one of the most attractive themes in contemporary science.[26–30] As a result, we wished to mimic DNA-like interactions to synthesize DNA heteronucleobase (T)-containing diblock copolymers by using a combination of nitroxide-mediated radical polymerization (NMRP) and click chemistry (Scheme 1). First, we employed NMRP to synthesize poly(styrene-*b*-vinylbenzyl chloride) (PS-*b*-PVBC) copolymers with various VBC lengths and then converted them to poly(styrene-*b*-4-vinylbenzyl azide) (PS-*b*-PVBN$_3$) copolymers through reactions with NaN_3. Finally, we used click chemistry to react PS-*b*-PVBN$_3$ with propargyl thymine (PT) to yield poly(styrene-*b*-4-vinylbenzyl triazolylmethyl methylthymine) (PS-*b*-PVBT) copolymers (Scheme 1), which we blended with the low-molecular-weight compound 9-hexadecyladenine (A-C16) to form self-assembly supramolecular structures, through strong complementary multiple hydrogen bonds, with two different length scales. We have used Fourier transform infrared (FTIR) spectroscopy, differential scanning calorimetry (DSC), small-angle X-ray scattering (SAXS), and transmission electron microscopy (TEM) to investigate these self-assembled supramolecular structures.

Experimental

Materials

Benzoyl peroxide, 2,2,6,6-tetramethyl-1-piperidinyloxy (TEMPO), styrene, and 4-vinylbenzyl chloride (Aldrich, USA) were passed through an alumina column and then vacuum-distilled from CaH_2 under reduced pressure prior to use. NaN_3 was purchased from Aldrich, USA. T, A, 1-bromohexadecane, and K_2CO_3 were purchased from Showa. Propargyl bromide (80% in toluene, stabilized with MgO) was purchased from Alfa. Copper(I) bromide (CuBr, 98%), *N*,*N*,*N*′,*N*″,*N*‴-pentamethyldiethylenetriamine (PMDETA, 99%) were purchased from Aldrich, USA. Dimethylsulfoxide (DMSO) and dimethylformamide (DMF) were distilled from CaH_2 under vacuum prior to use. 1-Hydroxy-2-phenyl-2-(2′,2′,6′,6′-tetramethyl-1-piperidinyloxy)ethane (TEMPO-OH) was synthesized as described previously.[31–33] All other chemicals were of reagent grade and used as received.

Propargyl-thymine (PT)

A solution of T (5.00 g, 40.1 mmol) and K_2CO_3 (8.30 g, 60.1 mmol) in DMF (100 mL) was fed into a 250 mL two-neck round-bottom flask equipped with an Ar inlet and a rubber septum and then cooled in an ice bath. After adding propargyl bromide (11.9 g, 100 mmol) dropwise to the solution, the mixture was stirred at room temperature overnight, the precipitate was filtered off, the solvent was evaporated, and the crude product was purified through column chromatography (*n*-hexane/EtOAc, 1 : 2) to obtain a pale-yellow powder (9.31 g, 85.0%). ^{1}H NMR ($CDCl_3$) δ_H: 1.96 (3H, *CH*$_3$), 2.48 (1H, propargyl *CH*), 4.55 (2H, *CH*$_2$–N), 7.30 (1H, thymine *H*-6), 9.21 (1H, *NH*). ^{13}C NMR ($CDCl_3$) δ_C: 11.82 [NCHC(*C*H$_3$)CO], 36.81 (CHC*C*H$_2$N), 75.13 (*C*HCCH$_2$N), 76.21 (CH*C*CH$_2$N), 110.96 [NCH*C*(CH$_3$)CO], 138.68 [N*C*HC(CH$_3$)CO], 150.36 (NH*C*ON), 164.06 (NH*C*OC).

9-Hexadecyladenine (A-C16)[34,35]

1-Bromohexadecane (2.44 g, 8.00 mmol) and anhydrous K_2CO_3 (1.08 g, 7.8 mmol) were added to a solution of A (1.00 g, 7.4 mmol) in DMF (50 mL) and then the resulting suspension was stirred at 60 °C for 48 h. The insoluble material obtained was filtered off, washed with water, and recrystallized twice from

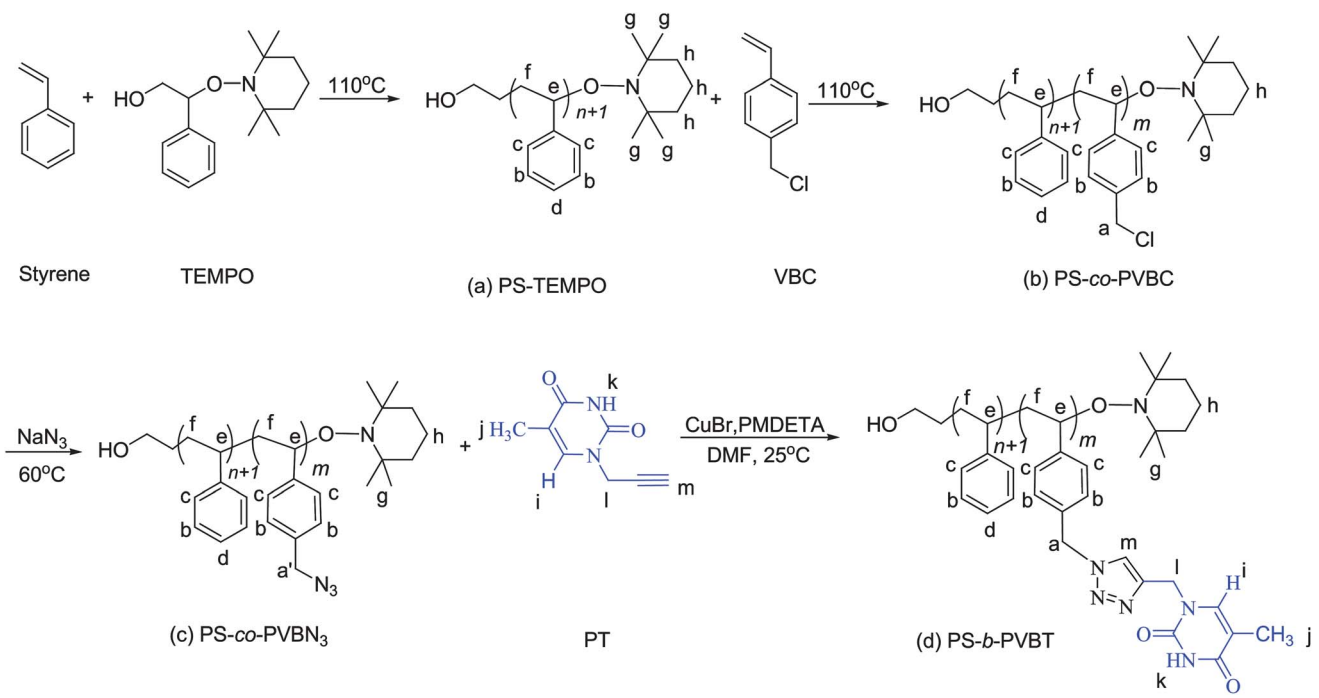

Scheme 1 Syntheses of (a) PS-TEMPO, (b) PS-*b*-PVBC, (c) PS-*b*-PVBN$_3$, and (d) PS-*b*-PVBT.

EtOH. ^{1}H NMR (500 MHz, d_6-DMSO, 25 °C, TMS): δ = 8.11 (2H; CH_2), 7.16 (2H; NH_2), 4.10 (2H; CH_2), 1.80–1.67 (2H; CH_2), 1.40–1.07 (26H; CH_2), 0.83 (3H; CH_3) ppm.

Polystyrene homopolymers (h-PS)[36]

Purified styrene (30 mL) and TEMPO-OH (47.7 mg) were placed in 50 mL three-neck flask. The orange reactant solution was heated at 95 °C for 3.5 h and then at 125 °C for several hours to obtain the h-PS sample, which was purified through repeated precipitations from CH_2Cl_2 into MeOH.

PS-*b*-PVBC

PS-*b*-PVBC copolymers with different contents of VBC units were prepared through bulk polymerization of 4-vinylbenzyl chloride (10 mL) in the presence of the macroinitiator h-PS (100 mg) at 125 °C for 24 h. The products were dissolved in THF and then poured into excess MeOH under vigorous agitation to precipitate a solid, which was collected by filtration and dried in a vacuum oven for 24 h to give PS-*b*-PVBC. ^{1}H NMR ($CDCl_3$) δ_H: 1.36 (1H, *CH*), 1.76 (2H, CH_2), 4.50 (2H, Ar–CH_2Cl), 6.52 (4H, PVBC *ArH*), 6.99 (5H, PS *ArH*). ^{13}C NMR ($CDCl_3$) δ_C: 40.25, 42.47 (CH_2CH_2Ar), 46.38 (Ar–CH_2Cl), 125.55, 128.59, 135.24, 145.16 (*Ar*).

PS-*b*-PVBN$_3$

NaN_3 (0.78 g, 11.9 mmol) was added to a solution of PS-*b*-PVBC (0.41 g, 2.43 mmol of VBC repeating units) in DMF (50 mL) and then the mixture was stirred overnight at room temperature and then precipitated into water. The product was redissolved in CH_2Cl_2 and reprecipitated from MeOH. The resultant solid was filtered off and dried in a vacuum oven for 24 h. ^{1}H NMR ($CDCl_3$) δ_H: 1.36 (1H, *CH*), 1.76 (2H, CH_2), 4.24 (2H, Ar-CH_2N_3), 6.52 (4H, PVBN$_3$ *ArH*), 6.99 (5H, PS *ArH*). ^{13}C NMR ($CDCl_3$) δ_C: 40.25, 42.47 (CH_2CH_2Ar), 54.37 (Ar–CH_2Cl), 125.55, 128.59, 135.24, 145.16 (*Ar*).

PS-*b*-PVBT

PS-*b*-PVBN$_3$ (0.42 g, 2.4 mmol of 4-vinylbenzyl azide repeating units), PT (8.1 mg, 0.49 mmol), and CuBr (2.4 mg, 0.16 mmol) were dissolved in DMF (50 mL) in a flask equipped with a magnetic stirrer bar. After one brief freeze–thaw–pump cycle, PMDETA (4.2 mg, 0.16 mmol) was added and then the mixture was carefully degassed through three freeze–thaw–pump cycles at 60 °C and stirred for 24 h. After passing through a neutral alumina column (to remove the copper catalyst) and pouring into excess EtOAc under vigorous agitation (to precipitate the block polymer), a brown solid was obtained. ^{1}H NMR (d_6-DMSO) δ_H: 4.87 (2H, NCHCCH_2N), 5.45 (2H, ArCH_2N), 6.29, 6.90 (9H, *ArH*), 7.54 (2H, ArCH$_2$N*CH*CCH$_2$N), 8.14 [1H, N*CH*C(CH$_3$)CO], 11.31 (1H, T *NH*). ^{13}C NMR (d_6-DMSO) δ_C: 11.82 [NCHC(*C*H$_3$)CO], 31.04, 42.43 (CH_2CH_2Ar), 36.10 (ArCH$_2$NCHCCH_2N), 52.63 (ArCH_2N), 109.14 [NCH*C*(CH$_3$)CO], 123.57 (ArCH$_2$N*C*HCCH$_2$), 127.53, 132.40, 150.89 (Ar), 141.20 [N*C*HC(CH$_3$)CO], 142.98 (ArCH$_2$NCH*C*CH$_2$), 162.44 (NH*C*ON), 164.73 (NH*C*OC).

Supramolecular complexes

DMF solutions containing different PS-*b*-PVBT/AC16 molar ratios were stirred for 6–8 h; the solvent was then evaporated slowly at room temperature for 24 h. The complex films were then dried at 50 °C for 2 days.

Characterization

^{1}H NMR spectra were recorded using a Varian Unity Inova 500 FT NMR spectrometer operated at 500 MHz, with $CDCl_3$ or d_6-DMSO as the solvent; chemical shifts are reported in parts per million (ppm). Molecular weights and molecular weight distributions were determined at 80 °C through gel permeation chromatography (GPC) using a Waters 510 HPLC equipped with a 410 differential refractometer, a UV detector, and three Ultrastyragel columns (100, 500, and 103 Å) connected in series; DMF was the eluent; the flow rate was 0.6 mL min^{-1}. The molecular weight calibration curve was obtained using polystyrene (PS) standards. FTIR spectra were recorded using a Bruker Tensor 27 FTIR spectrophotometer; 32 scans were collected at a spectral resolution of 1 cm^{-1}. The conventional KBr disk method was employed: the dissolved sample was cast onto a KBr disk and then dried under vacuum at 120 °C. Because polymers containing amino groups and C=O groups are hygroscopic, pure N_2 gas was used to purge the spectrometer's optical box to maintain the sample films' dryness. The glass transition (T_g) and melting (T_m) temperatures of the copolymer and complex films were determined through DSC using a TA Q-20 instrument; the scan rate was 20 °C min^{-1} within the temperature range 30–250 °C. The glass transitions were measured in the DSC sample cell after the sample (5–10 mg) had been cooled rapidly to −90 °C from the first scan. The glass transition temperature is defined herein as the midpoint of the heat capacity transition between the upper and lower points of deviation from the extrapolated liquid and glass lines. SAXS data were collected using the BL17A1 wiggler beamline of the National Synchrotron Radiation Research Center (NSRRC), Taiwan. The samples were sealed between two Kapton windows (thickness: 12 μm) and measured at room temperatures. An X-ray beam having a diameter of 0.5 mm and a wavelength (λ) of 1.1273 Å^{-1} was used for the SAXS measurements (Q range: 0.015–0.3 Å^{-1}). TEM experiments were conducted using a JEOL 2100 microscope (Japan) operated at 200 kV. Ultrathin sections of the samples were prepared using a Leica Ultracut S microtome equipped with a diamond knife. Slices (thickness: *ca.* 700 Å) were cut at room temperature. The ultrathin sections of the PS-*b*-PVBT/AC16 complexes were placed onto copper grids coated with carbon supporting films and then stained through exposure to the vapor of I_2, which is a preferential staining agent for PVBT and A-C16; in the micrographs, the PS-*b*-PVBT/AC16 and PS domains appeared dark and bright, respectively.

Results and discussion

Synthesis of PS-*b*-PVBC block copolymers

We added TEMPO-OH as the initiator for thermal bulk polymerization of the highly reactive PS and VBC monomers at high temperatures. Fig. 1(a) and (b) present ^{1}H NMR spectra of PS

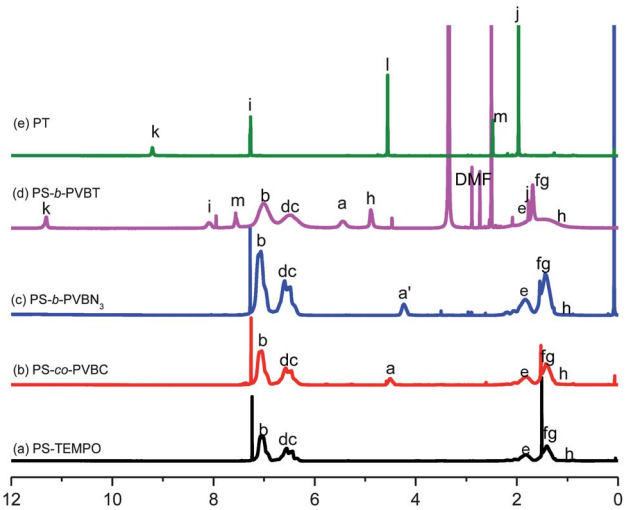

Fig. 1 ^{1}H NMR spectra of (a) PS-TEMPO, (b) PS-*b*-PVBC, (c) PS-*b*-PVBN$_3$ in $CDCl_3$, (d) PS-*b*-PVBT in d_6-DMSO, and (e) PT.

and PS-*b*-PVBC, respectively, in $CDCl_3$. The successful synthesis of the PS homopolymer was confirmed by the signals for the styrenic aromatic protons at 7.2 and 6.2–6.8 ppm; the signal near 0.9 ppm originated from the tetramethyl protons of the TEMPO-OH initiator. The tetramethyl signal is reported[37] to appear at 0.1–1.3 ppm as several peaks with variable intensities, due to conformational inversion involving ring conversion; herein, we used only the peak at 0.9 ppm to indicate attachment of the TEMPO unit. We prepared PS-*b*-PVBC copolymers from polymerizations of VBC with PS-TEMPO macroinitiators. Clearly, a signal for the chloromethyl protons at 4.5 ppm (CH_2Cl) of the PVBC block segment appeared in the spectrum of the PS-*b*-PVBC block copolymer in Fig. 1(b), providing evidence for its formation. We calculated the number-average molecular weight (M_n) of the PVBC block segment from the ^{1}H NMR spectrum of the copolymer based on the peak integration ratio of the signals of the benzene rings and chloromethyl groups. Similarly, a signal for the chloromethyl units (CH_2Cl) of the PVBC block segment appeared at 46.38 ppm in the ^{13}C NMR spectrum of the PS-*b*-PVBC block copolymer [Fig. 2(b)], providing additional evidence for its formation. Fig. 3 displays GPC traces of the PS-TEMPO macroinitiator and PS-*b*-PVBC; each reveals a narrow molecular weight distribution (<1.2). Block copolymers prepared from the PS-TEMPO macroinitiator resulted in products having narrow polydispersity and high symmetry, with monomodal GPC traces. The absence of the PS-TEMPO macroinitiator peak supports the formation of the PS-*b*-PVBC diblock copolymers, with the peak maxima of these traces clearly shifting to higher molecular weight upon increasing the ratio of VBC monomer to PS-TEMPO macroinitiator, confirming the successful syntheses of the PS-*b*-PVBC diblock copolymers.

Synthesis of PS-*b*-PVBN$_3$ block copolymers

Fig. 1(c) presents the ^{1}H spectrum of PS-*b*-PVBN$_3$ in $CDCl_3$. The resonance of the benzylic methylene groups shifted upfield significantly from 4.54 ppm for PS-*b*-PVBC [CH_2Cl, Fig. 1(b)] to 4.23 ppm for PS-*b*-PVBN$_3$ [CH_2N_3, Fig. 1(c)]. The absence of a resonance at 4.54 ppm suggested that the substitution reactions had occurred to completion, as confirmed by the ^{13}C NMR spectra, where the signal of the benzylic methylene units shifted downfield to 54.3 ppm [CH_2N_3 Fig. 2(b)] from 46.3 ppm [CH_2Cl, Fig. 2(c)], and by the presence of a characteristic signal for the azido groups at 2105 cm^{-1} in the FTIR spectrum of PS-*co*-PVBN$_3$ [Fig. 4(c)].

Synthesis of PT

We prepared PT through the substitution of propargyl bromide with T. The complete substitution of PT was confirmed in the ^{1}H NMR spectrum [Fig. 1(e)], in which the signal of the propargylic methylene group of propargyl bromide (4.60 ppm) shifted downfield (4.56 ppm) for PT. The lack of any remnant signal at 4.60 ppm suggested that the substitution reaction had reached completion. Fig. 4(e) displays the FTIR spectrum of PT, recorded at room temperature. The substitution of the Br atom with T led to the appearance of stretching vibration bands for the C≡C and ≡C–H groups at 2120 and 3254 cm^{-1}, respectively, with that of the C=O group of the T unit appearing at 1690 cm^{-1}, confirming that PT had been obtained.

Synthesis of PS-*b*-PVBT block copolymers

We synthesized PS-*b*-PVBT copolymers from the azide-functionalized block copolymers PS-*b*-PVBN$_3$ and PT *via* click reactions of vigorously stirred, concentrated solutions in DMF at room temperature, to which we added CuBr and PMDETA. After performing the azide/alkyne cycloadditions, the signal of the benzylic methylene groups of PS-*b*-PVBN$_3$ [CH_2N_3, 4.23 ppm ($CDCl_3$), Fig. 1(c)] shifted downfield significantly to 5.45 ppm for PS-*b*-PVBT in d_6-DMSO [Fig. 1(d)]. In addition, the signal for the propargylic CH_2 group of PT (4.56 ppm in $CDCl_3$) also shifted downfield to 4.88 ppm for PS-*b*-PVBT in d_6-DMSO, with the signal of the CH groups of the triazole units appearing at 7.53 ppm, confirming the successful synthesis of PS-*b*-PVBT. Fig. 1 summarizes all of the other peak assignments. We also used ^{13}C NMR spectroscopy to characterize the product of the click reaction (Fig. 2). The signal of the benzylic CH_2 groups of PS-*b*-PVBN$_3$ at 54.6 ppm [Fig. 2(c)] shifted to 52.67 ppm for PS-*b*-PVBT [Fig. 2(d)]. The signals of the alkyne carbon atoms of PT (74.8 and 76.0 ppm) were absent in the spectrum of PS-*b*-PVBT [Fig. 2(d)], but two new peaks appeared at 124.0 and 142.6 ppm [Fig. 2(d)], representing the carbon atoms of the triazole units, confirming the successful synthesis of PS-*b*-PVBT. In addition, the signal for the CH_2 group of PT at 36.3 ppm shifted to 35.5 ppm in the spectrum of PS-*b*-PVBT; meanwhile, the signals of the carbon atoms of the phenyl rings of the PT units appeared near 133 ppm, whereas the other phenyl ring carbon atoms resonated near 123.6 ppm. The signals of the C=O groups of the T moieties (N*C*ONH, NH*C*OCCH$_3$) appeared at 162.25 and 164.54 ppm, again confirming the successful synthesis of PS-*b*-PVBT. FTIR spectroscopic analysis (Fig. 4) confirmed the complete disappearance of the characteristic signals for the azido and acetylene groups. The signal at 2105 cm^{-1}, corresponding to the absorbance of the azido group of PS-*b*-PVBN$_3$, was absent in the spectrum of PS-*b*-PVBT; the absorption band of the C=O groups of the PT units appears at 1690 cm^{-1} in the spectra of the

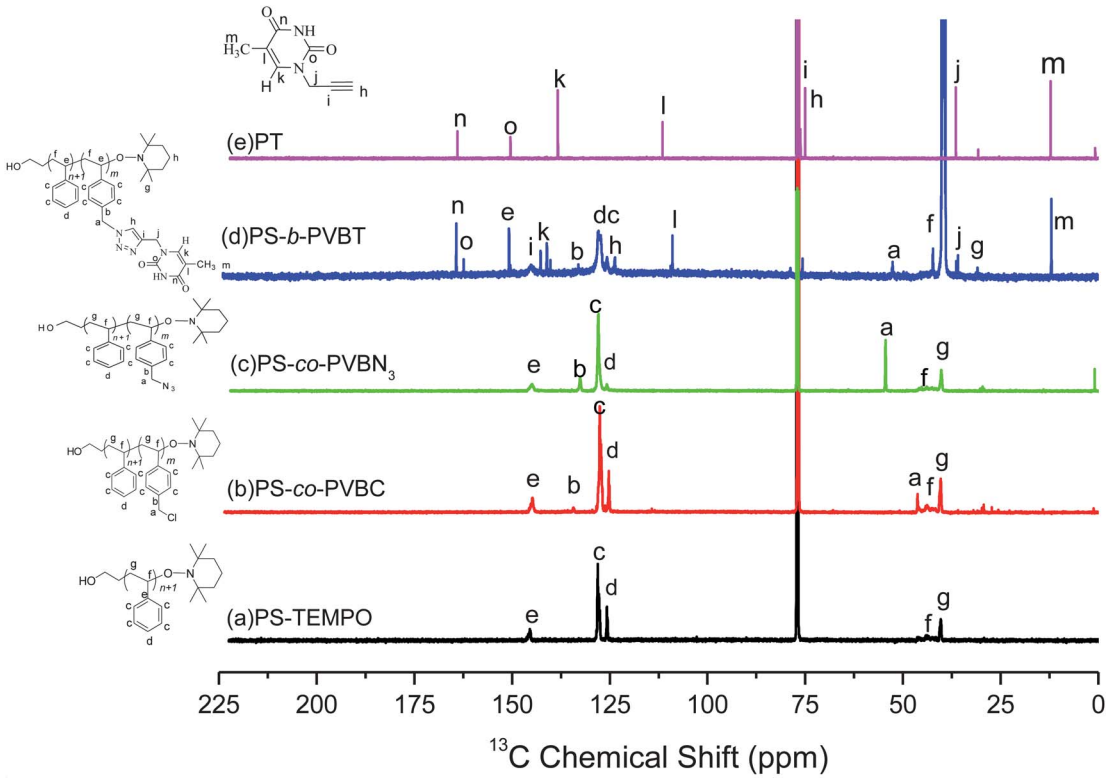

Fig. 2 ^{13}C NMR spectra of (a) PS-TEMPO, (b) PS-*b*-PVBC in $CDCl_3$, (c) PS-*b*-$PVBN_3$ in CDCl3, (d) PS-*b*-PVBT in d_6-DMSO, and (e) PT.

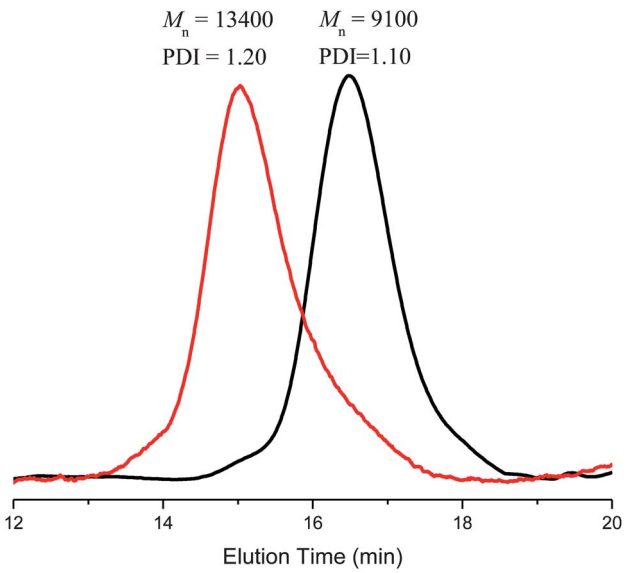

Fig. 3 GPC analyses of PS and PS-*b*-PVBC.

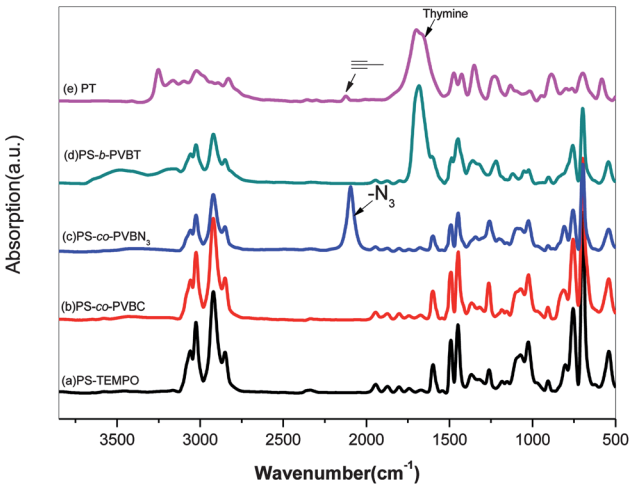

Fig. 4 FTIR spectra of (a) PS-TEMPO, (b) PS-*b*-PVBC, (c) PS-*b*-$PVBN_3$, (d) PS-*b*-PVBT, and (e) PT.

PS-*b*-PVBT copolymers, indicating that the azido and acetylene functionalities had participated in the click reactions. Taken together, the ^{1}H NMR and FTIR spectra confirmed the successful syntheses of PS-*b*-PVBT copolymers.

Thermal properties of PS-*b*-PVBT

Fig. 5 presents the thermal properties of the PS-*b*-PVBT diblock copolymers, determined from DSC analyses. Diblock copolymers normally exhibit two values of T_g when two different types of segments are present in the polymer chain. Our DSC measurement revealed that the lower-temperature glass transitions of the PS_{87}-*b*-$PVBT_{22}$ block copolymers occurred near 108 °C, indicating a large presence of PS segments. We assign the higher-temperature glass transitions to the PVBT segments in the copolymer (*ca.* 165 °C). Table 1 lists the molecular weights and thermal properties of the PS-*b*-PVBT copolymers used in this study, as determined through GPC, ^{1}H NMR spectroscopy, and DSC analyses.

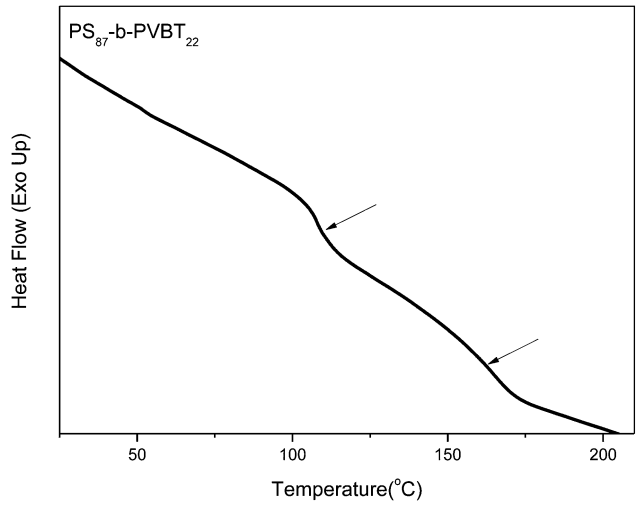

Fig. 5 DSC thermograms of the PS_{87}-*b*-$PVBT_{22}$ diblock copolymers.

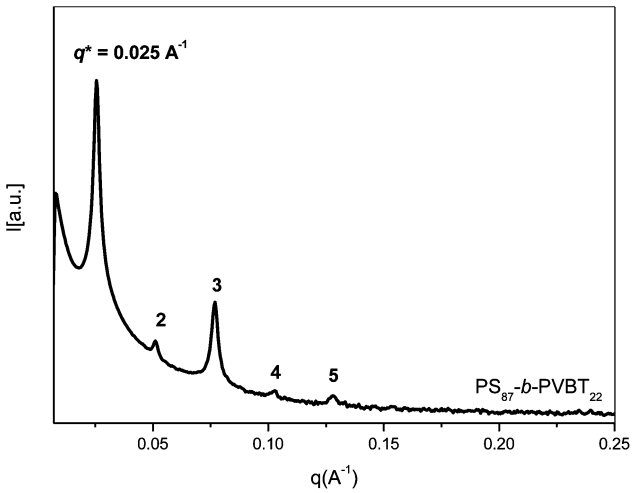

Fig. 6 SAXS patterns of the PS_{87}-*b*-$PVBT_{22}$ diblock copolymers.

Self-assembly of PS-*b*-PVBT

Fig. 6 displays the SAXS analysis data of the PS_{87}-*b*-$PVBT_{22}$, suggesting that the pure PS_{87}-*b*-$PVBT_{22}$ diblock copolymer featured a lamellar microdomain structure, judging from the positions of the high-order scattering maxima at the scattering vectors q of multiple integers relative to the position of the first-order scattering maximum ($q/q_m = 1, 2, 3, 4$, and 5). The couple of SAXS peaks located at positions of multiple q of 0.025 $Å^{-1}$ indicates a lamellar phase with a long period of 25.1 nm, extracted from the first peak position ($2\pi/q$). The pure PS_{87}-*b*-$PVBT_{22}$ diblock copolymer exhibited an alternating lamellar morphology and long-range-ordered pattern with a lamellar period of approximately 23 nm, as revealed in the TEM images in Fig. 7, consistent with the SAXS analysis data in Fig. 6. For a lamellar structure, the intensity of the n^{th} order peak is proportional to $\sin^2(\pi n\Phi_a)/n^2$), where Φ_a, equal to d_a/d, is the volume fraction of phase A; when the volume fractions of the two phases are equal, all even-order peaks are reduced to zero height.[38] Because the volume fraction of the PS segment for PS_{87}-*b*-$PVBT_{22}$ was approximately 0.64, which is close to 0.5, the intensities of even-order peaks (2 and 4q*) are small for this diblock copolymer.

Hierarchical self-assembly of supramolecular structures from PS-*b*-PVBT/A-C16 complexes

Synthesis of 9-hexadecyladenine (A-C16). 9-Hexadecyladenine was prepared through the substitution of 1-bromohexadecane with A. The FTIR spectrum of 9-hexadecyladenine reveals [Fig. 8(a)] bands at 3363 (free NH_2 stretching), 3282 (hydrogen-bonded NH stretching), and 2931 and 2875 cm^{-1} (aliphatic C–H stretching), as well as two strong bands at 1675 and 1602 cm^{-1} corresponding to bonded NH_2 scissor plus ring stretching and ring stretching plus bonded NH_2 scissor, respectively. The ^1H NMR spectrum of 9-hexadecyladenine reveals peaks at 4.18 (hexadecyl CH_2), 5.6 (NH_2 in A group), and 7.78 and 8.36 ppm (C=N).

Thermal properties of PS-*b*-PVBT/A-C16 complexes. The glass transition temperature is an important physical property reflecting changes in intermolecular interactions. Fig. 9 displays second-run DSC thermograms of PS_{87}-*b*-$PVBT_{22}$/A-C16 blends at different molar ratios. The two glass transitions of pure PS_{87}-*b*-$PVBT_{22}$ appeared at 108 and 165 °C, as mentioned previously. The melting and crystallization temperatures of A-C16 were approximately 123 and 93 °C, respectively. The repeat unit of PS_{87}-*b*-$PVBT_{22}$/A-C16 complexes, involving the somewhat-longer 9-hexadecyladenine, assumed full complexation at a PS_{87}-*b*-$PVBT_{22}$/A-C16 blend ratio of $1/x$, where x denotes a mixture of PS_{87}-*b*-$PVBT_{22}$ and A-C16 with x A-C16 molecules per repeat unit of PS_{87}-*b*-$PVBT_{22}$. For the PS_{87}-*b*-$PVBT_{22}$/A-C16 = 1/0.2 complex, we observed two values of T_g; we assign the lower (97 °C) to the PS-dominant phase, which had phase-separated from the PVBT/A-C16 complex, and the higher (140 °C) to the multiply hydrogen-bonded PVBT/A-C16 complex phase. The value of T_g of the complex phase was lower than that of the pure PVBT because of the presence of the side-chain alkyl groups of A-C16, which constituted a disordered phase, implying that highly complementary multiple hydrogen bonding was

Table 1 Characterization of PS-*b*-PVBT diblock copolymer used in this study

Sample	PS (M_n)[a]	PVBC (M_n)[a]	PS (M_n)[a]	PVBT (M_n)[a]	T_g (°C)[b]	T_g (°C)[b]	PDI[c]	f_{ps}[d]
PS_{87}-*b*-$PVBT_{22}$	9000	3300	9000	7400	108.8	164.9	1.20	0.64

[a] Obtained by ^1H NMR spectra, where n and m are repeat units of PS and PVBC. [b] Determined by DSC at 20 °C min^{-1}. [c] Obtained by GPC trace with DMF eluent of 0.6 mL min^{-1} and PS-standard calibration. [d] Volume fraction of PS block segment calculated from group contribution method (densities of PS and PVBT are 1.108 and 1.826 g cm^{-3}, respectively).[45]

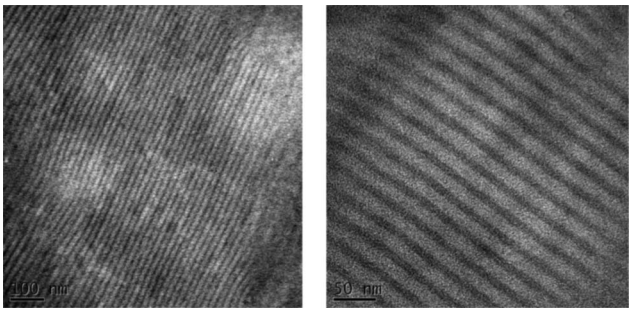

Fig. 7 TEM images of the diblock copolymer of PS_{87}-*b*-$PVBT_{22}$.

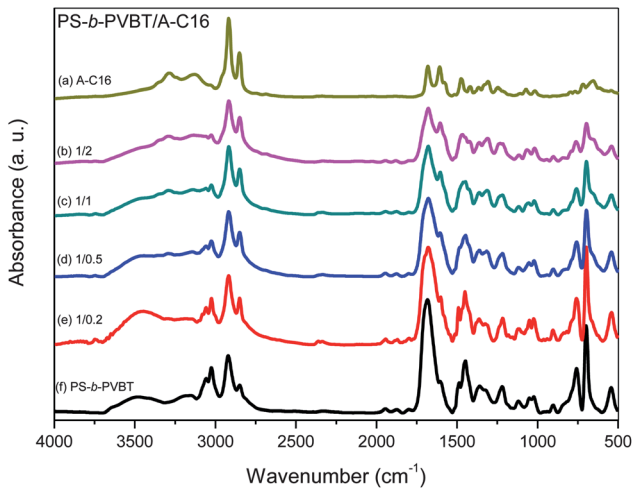

Fig. 8 FTIR spectra, recorded at room temperature, of PS_{87}-*b*-$PVBT_{22}$/A-C16 blends at different molar ratios.

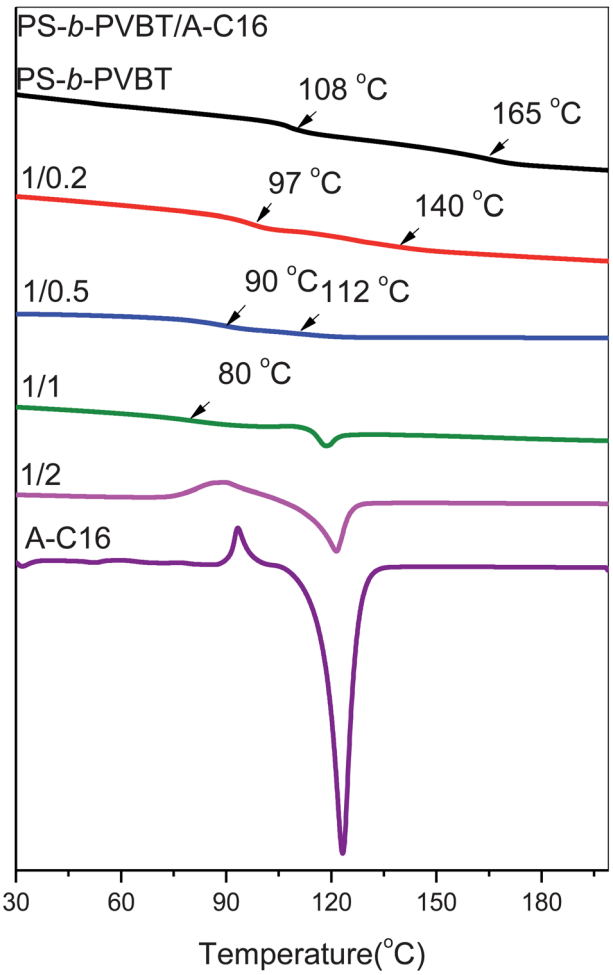

Fig. 9 DSC thermograms of PS_{87}-*b*-$PVBT_{22}$/A-C16 blends at different molar ratios.

occurring to form the PS-*b*-PVBT/A-C16 complexes.[39–44] Notably, the value of T_g of the PS segment in the complex was lower than that of the PS segment in the absence of A-C16, due to the more-flexible connection with the PVBT/A-C16 complex (T_g = 140 °C) compared with that of the pure PVBT segment (T_g = 165 °C). As a result, the PS_{87}-*b*-$PVBT_{22}$/A-C16 = 1/0.5 complex featured two values of T_g (90 and 112 °C, respectively). Again, we assign the lower- and higher-temperature glass transitions to the PS phase and PVBT/A-C16 miscible phase, respectively. For the PS_{87}-*b*-$PVBT_{22}$/A-C16 = 1/1 complex, we detected only a single, but broad, endothermic event near 80 °C. Here, we suspect that the glass transition of the miscible PVBT/A-C16 microphase had, by coincidence, dropped to the same temperature range as that of the PS segment, such that the two could not be resolved. In addition, we also found a value of T_m of 118 °C at this molar ratio, because the alkyl side-chains of A-C16 formed a more-regular crystalline phase, arranged perpendicularly to the amorphous sheets; crystallization of the alkyl tails occurred in sheets that separated the amorphous regions.[39–44] A further increase in the molar ratio to the PS_{87}-*b*-$PVBT_{22}$/A-C16 = 1/2 complex caused the value of T_m to shift significantly to 120 °C because of the presence of excess A-C16; no glass transition was observed at this ratio. This intriguing behavior led us to investigate the microstructures of these blends in more detail through SAXS and TEM characterization.

Infrared spectroscopy of PS-*b*-PVBT/A-C16 complexes. Infrared spectroscopy is a highly effective method for investigating multiple hydrogen bonding interactions in supramolecular polymer complexes.[45] It can be used as a tool to study, both qualitatively and quantitatively, the formation of multiple hydrogen bonds. The complementary multiple hydrogen bonding between PS_{87}-*b*-$PVBT_{22}$ and A-C16 is strong; at room temperature, equal numbers of T and A groups lead to nearly fully complexed comb copolymer-like systems.[46] The FTIR spectra in Fig. 8 confirm the existence of multiple hydrogen bonds between the PS_{87}-*b*-$PVBT_{22}$ and A-C16. The stretching of the free and hydrogen-bonded NH groups of the pure PS-*b*-PVBT appear as characteristic peaks at 3500 and 3172 cm^{-1}, respectively. The intensity of the free amide NH stretching vibration at 3500 cm^{-1} decreased upon increasing the amount of added A-C16, indicating that PS-*b*-PVBT associated strongly with its complement A-C16; the signal in the NH stretching region of the PS-*b*-PVBT and A-C16 mixture, where the band at 3500 cm^{-1} corresponds to free NH stretching, shifted to 3427 cm^{-1}, attributable to the A groups interacting with the T units.[46,47] In addition, a peak appeared at 3200 cm^{-1} that corresponded to the NH groups in the T units interacting with the A moieties.[48] Upon increasing the content of A-C16, we also

observed growing signals for the multiple hydrogen bonding interactions of the C═O groups of T units with the NH_2 groups of A units (at *ca.* 1649–1670 cm^{-1}) and for the pyridyl groups of A moieties interacting with the NH groups of T moieties (at *ca.* 1649–1670 cm^{-1}).[25] The expanded FTIR spectra (1500–1800 cm^{-1}) in Fig. 10 reveal signals for the free and hydrogen-bonded C═O groups of PVBT at 1706 and 1670 cm^{-1}, respectively, representing the T groups. The A groups of A-C16 provide characteristic peaks at 1680 and 1600 cm^{-1}, corresponding to NH bending and stretching of free pyridyl rings, respectively. We observed five major peaks by analyzing these spectra using the second-derivative technique, representing free C═O groups (1700–1710 cm^{-1}); self-complementary T···T multiple hydrogen bonding (1670–1680 cm^{-1}), intermolecular A···T multiple hydrogen bonding (*ca.* 1645–1655 cm^{-1}); free pyridyl and benzene ring stretching (1600–1610 cm^{-1}) of A-C16 and PS segments; and benzene ring stretching of PS segments (1570–1580 cm^{-1}). Here, we combined the multiple hydrogen bonding interactions between the C═O groups of T units and the NH_2 groups of A units with those of the pyridyl groups of A units interacting with NH groups of T units (*ca.* 1645–1655 cm^{-1}). We combined all five of these absorption peaks to represent multiple hydrogen bonding interactions in PS-*b*-PVB/A-C16 complexes because in many bands it was difficult to calculate the quantitative area fraction of each peak. Additionally, we focused only on the fractions of free T groups in the PS-*b*-PVB/A-C16 complexes. For deconvolution, we fitted a series of Gaussian distributions to quantify the fractions of each of the peaks displayed in Fig. 10. The fractions of free C═O groups of the T units in PVBT decreased upon increasing the A-C16 content (inset to Fig. 10), indicating the existence of multiple hydrogen bonding interactions between the A and T groups.

SAXS and TEM analyses of PS-*b*-PVBT/A-C16 complexes. Fig. 11 presents room-temperature SAXS profiles of PS-*b*-PVBT/A-C16 complexes at different molar ratios, recorded to confirm their self-assembled supramolecular structures. In the lower-*q* region, SAXS analysis revealed the lamellar microdomain structure of the pure PS-*b*-PVBT diblock copolymer, judging from the scattering maxima at relative positions of 1 : 2 : 3 : 4 : 5, corresponding to a domain spacing of 25.0 nm, that was associated with the larger-scale copolymer domain structure arising from microphase separation of the PS and PVBT blocks. In the higher-*q* region for the PS-*b*-PVBT/A-C16 complex, we could discern the formation of smaller-scale lamellar mesophases organized by the PVBT/A-C16 comb blocks. Pure A-C16 shows two peaks due to the crystal structure

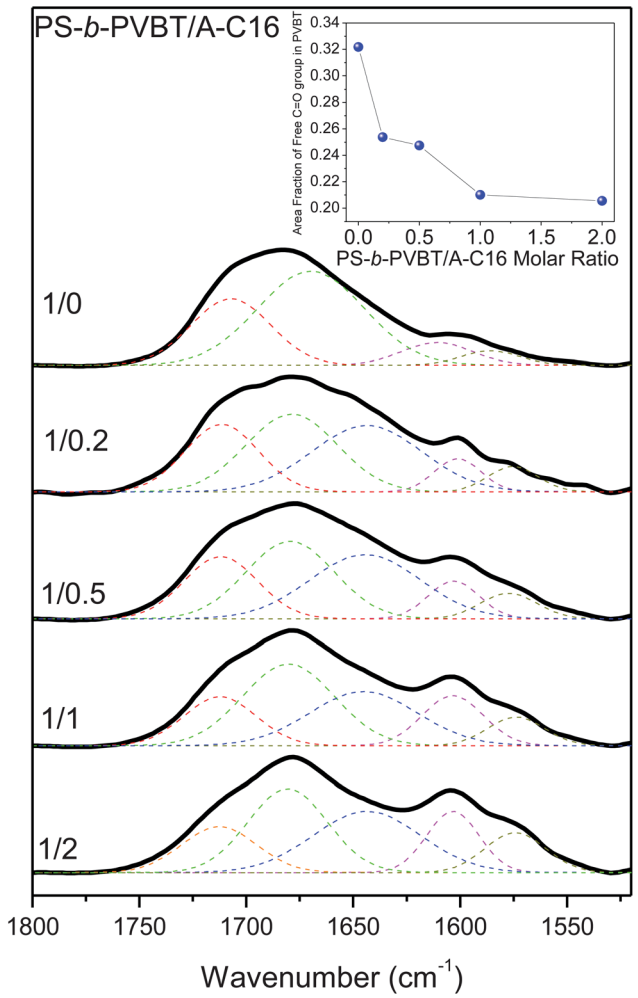

Fig. 10 Data from curve-fitting of the room-temperature FTIR spectra of PS_{87}-*b*-$PVBT_{22}$/A-C16 blends at different molar ratios.

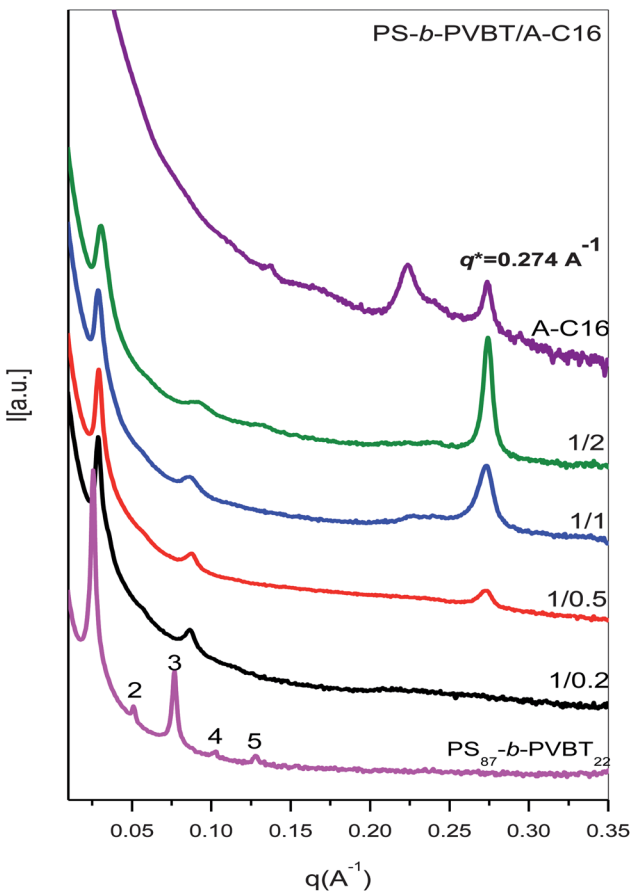

Fig. 11 SAXS patterns of PS_{87}-*b*-$PVBT_{22}$/A-C16 complexes at different molar ratios.

that would also occur in a bulk sample. A scattering peak was observed at a higher value of q of 0.274 Å^{-1}, with an interlamellar distance of 2.29 nm from C16. In addition, at lower value of 0.224 Å^{-1} with the d-spacing of 2.80 nm would come from the length of A-C16. The system with PS-*b*-PVBT/A-C16 = 1/2 provided a scattering peak at a value of q of 0.274 Å^{-1}, with an interlamellar distance of 2.29 nm. This scattering peak broadened at lower values of x because of the poorer coherent order of the lamellar stacks. In addition, the interlamellar distance increased slightly upon decreasing the value of x.[49] The structure in PS-*b*-PVBT/A-C16 complex is different from that in pure A-C16 (the lower value of 0.224 Å^{-1} disappeared), suggesting that hydrogen bonding is significant. In addition, the crystallization forces may also be quite large compared with the hydrogen bonding forces, and would dominate. As a result, PVBT/A-C16 complex that crystallizes and hydrogen bonding would still be present as the two materials would still be in contact. In the lower-q region for the PS-*b*-PVBT/A-C16 complex, the SAXS traces of all of complexes featured at least one higher-order reflection at a value of the scattering vector q of 3 relative to the position of the first-order scattering maximum, indicating a lamellar morphology. The intensities of the even-order peaks were gradually suppressed upon increasing the A-C16 content, implying that the volume fractions of the PVBT/A-C16 and PS phases were almost equal. For example, the volume fractions of the PS phases in the lamellar structures decreased to close to 52% in PS-*b*-PVB/A-C16 = 1/0.5 and 44% in PS-*b*-PVB/A-C16 = 1/1 because the A-C16 units were solubilized within the PVBT domains. In addition, the first-order scattering position obviously shifted to the higher-q region upon increasing the A-C16 content, indicating that the interlamellar spacing (D) decreased accordingly, similar to our previous findings for poly(styrene-*b*-vinylphenol)/P4VP blends that interact through strong single-site hydrogen bonding interactions.[50] Fig. 12(a) and (b) present TEM images of the PS-*b*-PVB/A-C16 = 1/1 complex stained with both

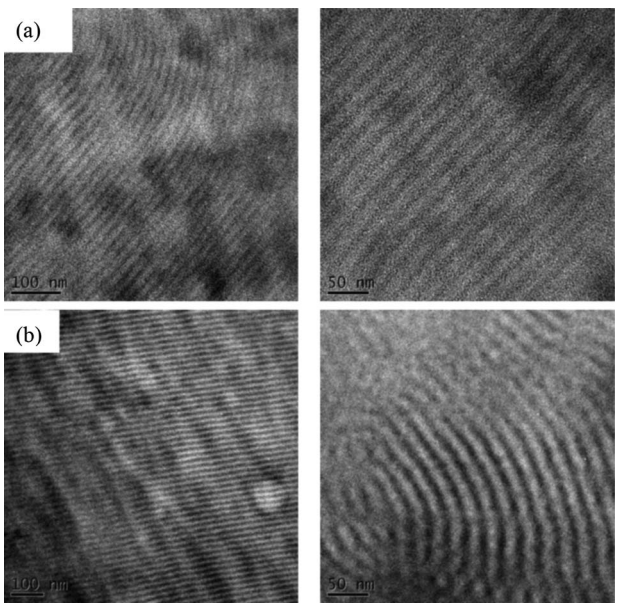

Fig. 12 TEM images of PS_{87}-*b*-$PVBT_{22}$/A-C16 = 1/0.5 stained with (a) both OsO_4 and I_2 and (b) only I_2.

OsO_4 and I_2, because OsO_4 interacts preferentially with both the PS and PVBT domains, whereas I_2 interacts preferentially only with the pyridyl group of A-C16 in the PVBT/A-C16 complex. We observe an alternating lamellar morphology and a long-range-ordered pattern having a lamellar period of approximately 20 nm, supporting the notion that the interlamellar spacing (D) decreased upon increasing the A-C16 content, consistent with the SAXS analysis data in Fig. 11. For Fig. 12(c) and (d), we stained the PVBT/A-C16 complex only with I_2, to enhance the contrast; in this case, the PS layers appear white and the PVBT/A-C16 layers dark. For the PS-*b*-PVB/A-C16 = 1/1 complex, the contrast was enhanced and we observed a long-range-ordered pattern having a lamellar period of approximately 20 nm. Here, we expected the supramolecular comb-like blocks to undergo two length-scales of self-assembly on the length scales of the block copolymer (long) and amphiphile (short), providing lamellar-within-lamellar structures (Scheme 2) for the PS_{87}-*b*-$PVBT_{22}$/A-C16 complexes. It has been established that polymer/amphiphile (PVBT/A-C16 in this case) layers are aligned perpendicular with respect to the microphase separation of block copolymers.[17–21]

We were also interested in examining how the A-C16 molecules were distributed in this complex. From considerations of volume fractions, the thickness of the PS layer in pure PS_{87}-*b*-$PVBT_{22}$ was 16.3 nm; this value decreased upon increasing the A-C16 content, such that the PS layer in PS_{87}-*b*-$PVBT_{22}$/A-C16 = 1/0.5 had a thickness of 11.4 nm. Furthermore, the correlated changes in the average distance a_J of the chemical junctions along the interface—and, therefore, the relative changes a_J/a_{J0} (where a_{J0} is for the pure block copolymer)—can be derived for the complexes. Simple volumetric conservation leads to

$$D/D_0 = (\rho_J/\rho_{J0})\Phi_{block}{}^{-1}$$

for a lamellar structure, where ρ_J is the number of block chains per unit interfacial area (*ca.* $a_J{}^2$), and, therefore, a_J/a_{J0} is approximately equal to $(\rho_J/\rho_{J0})^{-1/2}$,[51,52] and Φ is the volume fraction of the block copolymer in the complex, as suggested by Hashimoto *et al.*[53] Based on these relations, we found that the values of a_J/a_{J0} for our complexes increased from 1.11 to 1.21 to 1.33 upon increasing the A-C16 content (x = 0.2, 0.5, and 1.0, respectively). The PS_{87}-*b*-$PVBT_{22}$/A-C16 complexes, characterized to feature complementary multiple hydrogen bonding, exhibited a decreasing interlamellar distance (*i.e.*, $D/D_0 < 1$), accompanied by an expansion in a_J ($a_J/a_{J0} > 1$). We surmise that the additive A-C16 could intervene in the PVBT chains of the block copolymer through complementary multiple hydrogen bonding at the interfaces, resulting in the observed expansion in a_J. The PS blocks, being chemically linked to the PVBT blocks, had to contract to accommodate the expanded interface zone. Consequently, the thickness of the PS layer and the lamellar spacing both decreased upon increasing the content of A-C16, as also shown in Scheme 2. In addition, we also could expect that the bound A-C16/PVBT complex simply has a reduced enthalpic cost at the interface. This is commonly observed with the addition of nanoparticles—they increase the interface per chain by 'hiding' the blocks from each other. Here, we ignore the possibility that the A-C16 is simply forming a crystal lamella and phase separating along the PVBT–PVBT interface. Fig. 13(a) displays temperature-dependent SAXS data for the

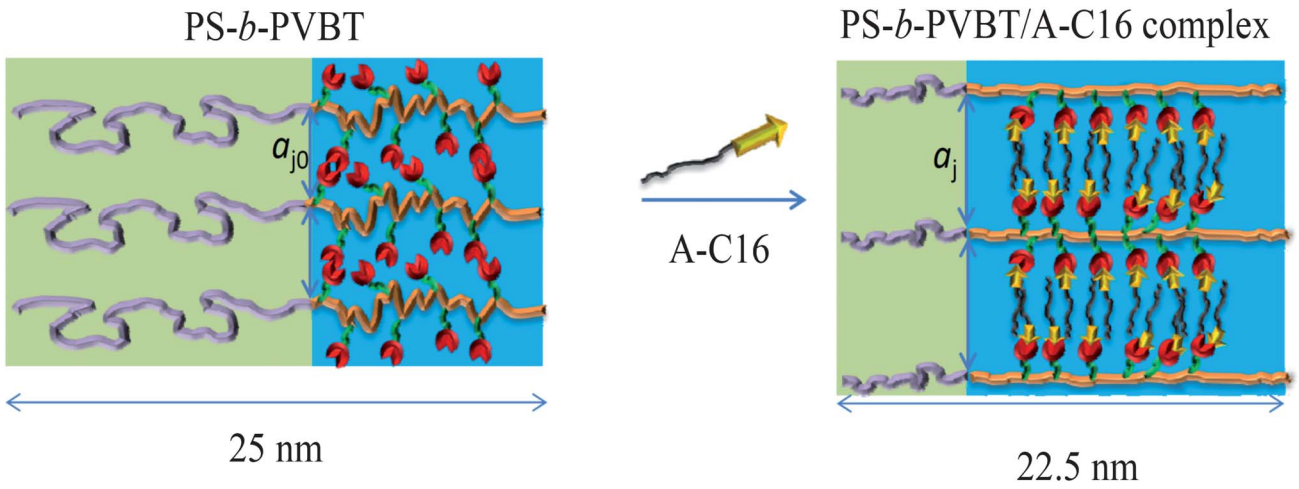

Scheme 2 Cartoon representation of lamellar-in-lamellar structure, featuring a short-length-scale lamellar order (PVBT/A-C16 complex) within a long-scale order consisting of PVBT-containing domains in a PS matrix.

PS-*b*-PVBT/A-C16 = 1/0.5 comb–coil block copolymer. A small peak at a value of q of 0.274 $Å^{-1}$ corresponds to the small length scale, having an interlamellar distance of 2.29 nm, noted in Fig. 11. This peak was not observable at 130 °C, which is higher than the melting temperature of A-C16, as indicated in Fig. 9. The lamellar-within-lamellar structure is confirmed by the

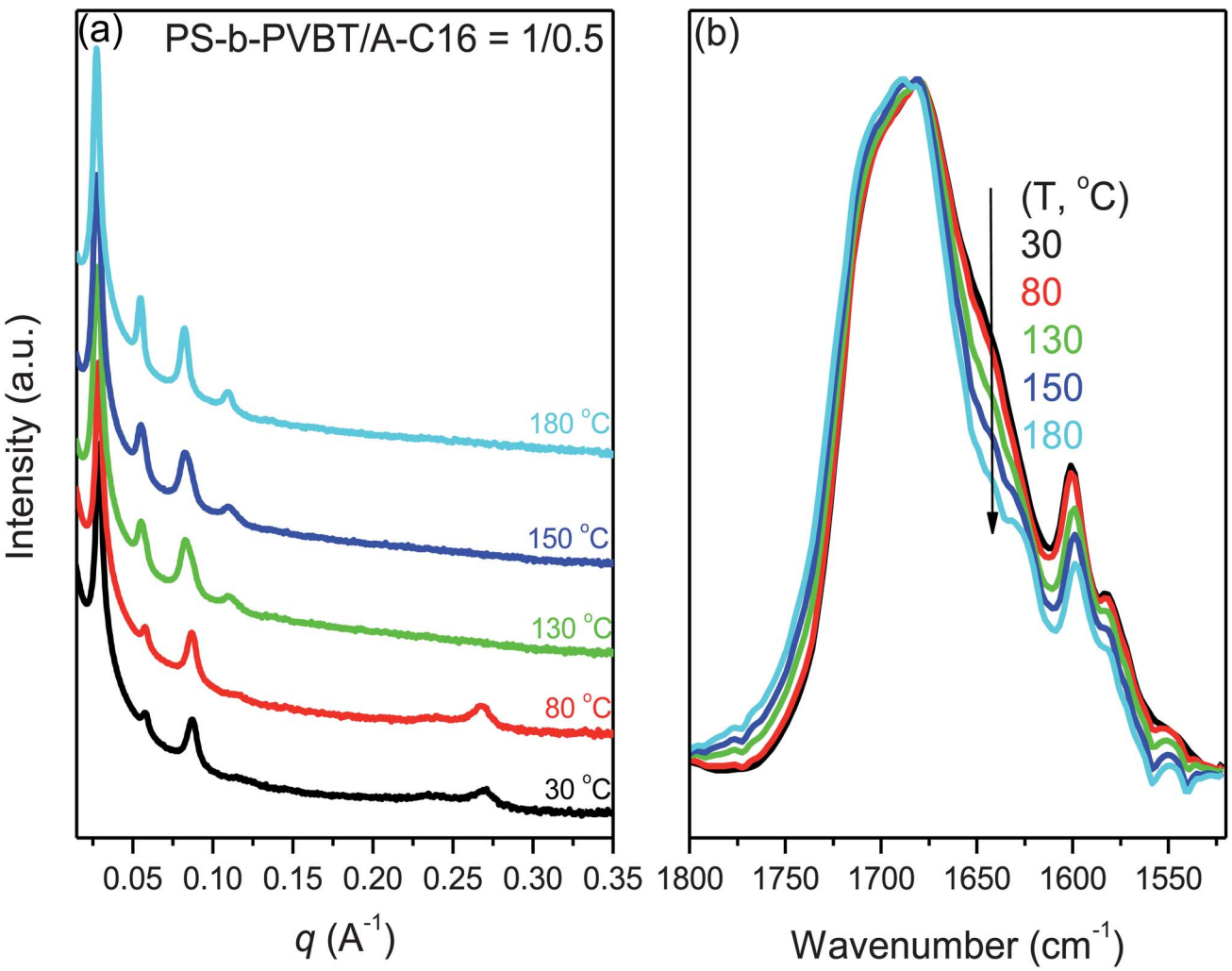

Fig. 13 (a) SAXS patterns and (b) FTIR spectra of PS_{87}-*b*-$PVBT_{22}$/A-C16 = 1/0.5, recorded at different temperatures.

occurrence of a SAXS peak at a value of q of 0.029 Å^{-1} with second-, third-, and fourth-order peaks, indicating lamellar order with a long period of 21.6 nm. Because the volume fractions of both layers were approximately the same ($f_{PS}^{v} = 0.52$), the second- and fourth-order peaks in the corresponding SAXS data were, therefore, systematically small. The second- and fourth-order peaks did, however, become apparent upon increasing the temperature, especially to values higher than 120 °C. The main reason for this behavior is that, at room temperature, A-C16 forms multiple hydrogen bonded interactions with PVBT and is not miscible in PS. Upon heating, the hydrogen bonds are gradually broken and, when the temperature reaches 120 °C, A-C16 becomes miscible with both PS and PVBT, similar to the behavior of PS-*b*-P4VP/PDP system,[54] as revealed in Scheme 3. As a result, the volume fraction of the PS domain ($f_{PS}^{v} > 0.52$) increased upon increasing the temperature of the PS-*b*-PVBT/A-C16 = 1/0.5 comb–coil block copolymer system, causing the second- and fourth-order peaks to become more intense than they were at room temperature.[38] We also used variable-temperature FTIR spectroscopy to confirm the gradually breaking of hydrogen bonds upon heating. Fig. 13(b) reveals that the fraction of multiple hydrogen bonding interactions of the C=O group of the T units with the NH_2 groups of the A units (signal at *ca.* 1649–1670 cm^{-1}) decreased upon increasing the temperature.

Conclusions

We have successfully synthesized T-containing diblock copolymers through a combination of NMRP and click chemistry. Strong complementary multiple hydrogen bonds formed between the PVBT and A-C16 units, resulting in a lamellae-within-lamellae two length-scales self-assembled structure, with PS lamellar domains (diameter: *ca.* 20–25 nm) in a matrix consisting of the lamellar mesophase (lamellar inter-distance: *ca.* 2.3 nm) organized by the PVBT/A-C16 complex, as evidenced through SAXS and TEM analyses. The A-C16 units could intervene in the PVBT chains of the block copolymer through complementary multiple hydrogen bonding at the interfaces, resulting in the observed expansion in the average distance of the chemical junctions along the interface, with the PS blocks, being chemical linked to the PVBT blocks, having to contract to accommodate the expanded interface zone. Consequently, the thickness of the PS layer and the lamellar spacing both decreased upon increasing the content of A-C16. Here, we have demonstrated another method through which multiple hydrogen bonding interactions can be used to obtain hierarchical self-assembled structures using supramolecular concepts.

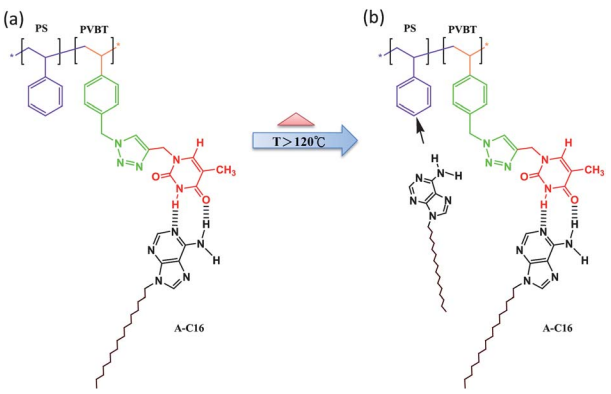

Scheme 3 (a) At room temperature, A-C16 is hydrogen bonded to PVBT and is not soluble (miscible) in PS. Upon heating the hydrogen bonds are gradually broken. (b) At $T >$ *ca.* 120 °C, A-C16 becomes soluble also in PS; *i.e.*, A-C16 exists in both the PVBT and PS domains.

Acknowledgements

This study was supported financially by the National Science Council, Taiwan, Republic of China, under contracts NSC 100-2221-E-110-029-MY3 and NSC 100-2628-E-110-001.

Notes and references

1 J. A. A. W. Elemans, A. E. Rowan and R. J. M. Nolte, *J. Mater. Chem.*, 2003, **13**, 2661–2670.
2 Y. He, T. Ye, M. Su, C. Zhang, A. E. Ribbe, W. Jiang and C. Mao, *Nature*, 2008, **452**, 198–201.
3 J. Ruokolainen, M. Saariaho, O. Ikkala, G. T. Brinke, E. L. Thomas, M. Torkkeli and R. Serimaa, *Macromolecules*, 1999, **32**, 1152–1158.
4 J. Rodriguez-Hernandez, F. Checot, Y. Gnanou and S. Lecommandoux, *Prog. Polym. Sci.*, 2005, **30**, 691–724.
5 Y. Matsushita, *Macromolecules*, 2007, **40**, 771–776.
6 Y. Matsushita, A. Takano, K. Hayashida, T. Asari and A. Noro, *Polymer*, 2009, **50**, 2191–2203.
7 W. C. Chen, S. W. Kuo and F. C. Chang, *Polymer*, 2010, **51**, 4176–4184.
8 G. Li, L. Shi, R. Ma, Y. An and N. Huang, *Angew. Chem., Int. Ed.*, 2006, **45**, 4959–4962.
9 S. W. Kuo, P. H. Tung, C. L. Lai, K. U. Jeong and F. C. Chang, *Macromol. Rapid Commun.*, 2008, **29**, 229–233.
10 C. H. Hsu, S. W. Kuo, J. K. Chen, F. H. Ko, C. S. Liao and F. C. Chang, *Langmuir*, 2008, **24**, 7727–7734.
11 S. W. Kuo, P. H. Tung and F. C. Chang, *Eur. Polym. J.*, 2009, **45**, 1924–1935.
12 X. Liu, M. Jiang, S. Yang, M. Chen, D. Chen, C. Yang and K. Wu, *Angew. Chem., Int. Ed.*, 2002, **41**, 29503.
13 X. Yan, G. Liu, J. Hu and C. G. Willson, *Macromolecules*, 2006, **39**, 1906–1912.
14 J. F. Gohy, S. K. Varshney and R. Jerome, *Macromolecules*, 2001, **34**, 3361–3366.
15 A. Harada and K. Kataoka, *Science*, 1999, **283**, 65–67.
16 J. F. Gohy, H. Hofmeier, A. Alexeev and U. S. Schubert, *Macromol. Chem. Phys.*, 2003, **204**, 1524–1530.
17 G. T. Brinke, J. Ruokolainen and O. Ikkala, *Adv. Polym. Sci.*, 2007, **207**, 113–177.
18 G. T. Brinke and O. Ikkala, *Chem. Rec.*, 2004, **4**, 219–230.
19 O. Ikkala and G. T. Brinke, *Science*, 2002, **295**, 2407–2409.
20 O. Ikkala and G. T. Brinke, *Chem. Commun.*, 2004, 2131–2137.
21 J. Ruokolainen, G. T. Brinke and O. Ikkala, *Adv. Mater.*, 1999, **11**, 777–780.
22 J. R. Smith, *Prog. Polym. Sci.*, 1996, **21**, 209–253.
23 S. W. Kuo and R. S. Cheng, *Polymer*, 2009, **50**, 177–188.
24 S. W. Kuo and S. T. Tsai, *Macromolecules*, 2009, **42**, 4701–4711.
25 Y. C. Wu and S. W. Kuo, *J. Mater. Chem.*, 2012, **22**, 2982–2991.
26 F. Ilhan, M. Gray and V. M. Rotello, *Macromolecules*, 2001, **34**, 2597–2601.
27 K. E. Feldman, M. J. Kade, T. F. A. De Greef, E. W. Meijer, E. J. Kramer and C. J. Hawker, *Macromolecules*, 2008, **41**, 4694–4700.
28 M. Seo, B. J. Beck, J. M. J. Paulusse, C. J. Hawker and S. Y. Kim, *Macromolecules*, 2008, **41**, 6413–6418.
29 S. Sivakava, J. Wu, C. J. Campo, P. J. Mather and S. J. Rowan, *Chem.–Eur. J.*, 2006, **12**, 446–456.
30 G. M. L. V. Gemert, J. W. Peeters, S. H. M. Sontjens, H. M. Janssen and A. W. Bosman, *Macromol. Chem. Phys.*, 2012, **213**, 234.
31 S. C. Chan, S. W. Kuo, C. H. Lu, H. F. Lee and F. C. Chang, *Polymer*, 2007, **48**, 5059–5068.

32 C. H. Lu, C. F. Huang, S. W. Kuo and F. C. Chang, *Macromolecules*, 2009, **42**, 1067–1078.
33 W. C. Chen, S. W. Kuo, C. H. Lu and F. C. Chang, *Macromolecules*, 2009, **42**, 3580–3590.
34 M. Souvik, M. G. Swetha, G. Debanjan, D. G. Gagan, M. Satyajit and K. Yamuna, *Nat. Nanotechnol.*, 2009, **4**, 325–330.
35 C. C. Cheng, C. F. Huang, Y. C. Yen and F. C. Chang, *J. Polym. Sci., Part A: Polym. Chem.*, 2008, **46**, 6416–6423.
36 W. H. Ting, S. A. Dai, Y. F. Shih, I. K. Yang, W. C. Su and R. J. Jeng, *Polymer*, 2008, **49**, 1497–1505.
37 S. H. Kim, Y. C. Park, G. H. Jung and C. G. Cho, *Macromol. Res.*, 2007, **15**, 587–594.
38 R. J. Roe, *Methods of X-ray and Neutron Scattering in Polymer Science*, Oxford University Press, New York, 2000.
39 F. Edmund, E. F. Jr Jordan, D. W. Feldeisen and A. N. Wrigley, *J. Polym. Sci., Part A-1*, 1971, **9**, 1835–1851.
40 M. Ballauff, *Makromol. Chem. Rapid Commun.*, 1986, **7**, 407–414.
41 M. Ballauff and G. F. Schmidt, *Makromol. Chem. Rapid Commun.*, 1987, **8**, 93–97.
42 S. Zhou, Y. Zhao, Y. Cai, Y. Zhou, D. Wang, C. C. Han and D. Xu, *Polymer*, 2004, **45**, 6261–6268.
43 K. Inomata, Y. Sakamaki, T. Nose and S. Sasaki, *Polym. J.*, 1996, **28**, 986–991.
44 K. Inomata, Y. Sakamaki, T. Nose and S. Sasaki, *Polym. J.*, 1996, **28**, 992–999.
45 M. M. Coleman, J. F. Graf and P. C. Painter, *Specific Interactions and the Miscibility of Polymer Blends*, Technomic, Lancaster, PA, 1991.
46 F. H. Beijer, R. P. Sijbesma, J. A. J. M. Vekemans, E. M. Meijer, H. Kooijman and A. L. Spek, *J. Org. Chem.*, 1996, **61**, 6371–6380.
47 Y. Kyogoku, R. C. Lord and A. Rich, *J. Am. Chem. Soc.*, 1967, **89**, 496–504.
48 F. H. Beijer, H. Kooijman, A. L. Spek, R. P. Sijbesma and E. W. Meijer, *Angew. Chem., Int. Ed.*, 1998, **37**, 75–78.
49 J. Ruokolainen, G. T. Brinke and O. Ikkala, *Macromolecules*, 1996, **29**, 3409–3415.
50 S. C. Chen, S. W. Kuo, U. S. Jeng and F. C. Chang, *Macromolecules*, 2010, **43**, 1083–1092.
51 E. Kim, H. Ahn, D. Y. Ryu, W. Joo, J. K. Kim, J. Jung and T. Chang, *Macromolecules*, 2008, **41**, 9875–9881.
52 T. Hashimoto, H. Tanaka and H. Hasegawa, *Macromolecules*, 1990, **23**, 4378.
53 T. Tanaka, H. Hasegawa and T. Hashimoto, *Macromolecules*, 1991, **24**, 240–251.
54 S. Valkama, T. Ruotsalainen, A. Nyka1nen, A. Laiho, H. Kosonen, G. T. Brinke, O. Ikkala and J. Ruokolainen, *Macromolecules*, 2006, **39**, 9327–9933.